PUAKO notes #03:
PSF reconstruction facility

O. Beltramo-Martin*

January 6, 2021

Contents

1 Rationale

The very core of the PSF reconstruction algorithm is implemented into the *psfReconstruction* object. This latter is designed to absorb the *telemetry* object and perform the 2D PSF reconstruction as well as the estimation of PSF figures of merits, such as the Strehl-ratio or FWHM. I detail in this document all the steps performed by the code to achieve a the reconstruction, with a scope on how each phase structures function calculations are implemented, including the anisoplanatism model. I also present simulation results and an analysis of the current PSF reconstruction performance in both NGS and LGS mode by comparing with NIRC2 images.

*olivier.beltramo-martin@lam.fr

2 The psfReconstruction class

The *psfReconstruction* class is called this way

```
psfr = psfReconstruction(trs,'fov',trs.cam.resolution+4,'flagToeplitz',true,
'flagNoiseMethod','autocorrelation','flagAnisoMethod','oomao','flagDphiMethod','Vii',
'addStatModes',{[]},'fitbg',false)
```

where *trs* is required the *telemetry* object instantiated by the user or directly by using the PUAKO property `trs`. Optional parameters are:

- `fov` is the field on view in pixels on which the PSF is reconstructed. By default, it is set up to the sky PSF resolution increased by 4 pixels for recentering purpose. Note that choosing such a value does introduce numerical aliasing due to the FFT algorithm. The impact is really weak, but if one tests this algorithm on simulated data without image noise, we would see the aliasing of diffraction effects. To get rid of this, I recommend to reconstruct the PSF over twice the support it must compared with simulated images.
- `flagToeplitz` is set to true to perform a faster reconstruction assuming the residual phase is stationary across the pupil. If set to false, the algorithms calculates the PSF in a 4D fashion [22, 2], although it has not been deeply tested so far. In practice, the stationarity assumption is accurate enough to not limiting the reconstruction quality.
- `flagNoiseMethod` is the method identity used for the noise estimation. By default, it is set up to 'autocorrelation, but the user can also choose 'theoretical' or 'rtf' options if we want to deploy another method than the one chosen during the instantiation of the *telemetry* object.
- `flagAnisoMethod` refers to the method to estimate the anisoplanatism structure function (angular-focal and tip-tilt), which is 'oomao' (default) based on covariance matrices calculations [5] or 'flicker' to choose the R. Flicker's model [8].
- `flagDphiMethod` refers to the method used to calculate the residual phase structure function set to 'Vii' by default [9], 'Uij' [21] or 'zonal'/'zonal_hr' to derive the point-wise OTF [10].
- `addStatModes` is a cell object, empty by default, that carries the coefficients in nm and the mode we want to add as static aberrations in the telescope OTF derivation, on top of calibrated NCPA, high-order and field-dependent static aberrations. For instance, setting

  ```
  Zer = zernike_puako([4,5],trs.tel.resolution);
  psfr = psfReconstruction(trs,'addStatModes',{[100,100], Zer.modes})
  ```

  allows to include a focus and an astigmatism static terms with 100 nm of rms value each. The user can include any type of modes and mix different nature of modes.
- `fitbg` is a boolean (false is default) that, if set to true, requests PUAKO to adjust a constant background value when scaling the reconstructed PSF over the focal-plane image.

As similarly as for the *telemetry* object, the user can define the `psfr` field of PUAKO by calling the function *p.getRecPSF* as follows

```
p = puako('path_imag',path_imag,'path_trs',path_trs,'path_calibration',path_calib);
p.getRecPSF({'n0004'},'fov',2*trs.cam.resolution,'fitbg',true)
p.psfr
```

PUAKO will automatically instantiate the *telemetry* object in which will be performed the noise and seeing estimations (see PUAKO note #02) before getting through the reconstruction. Eventually, the user can play with the reconstructed PSFs (psfr.rec_), as well as all OTFs (psfr.otf), phase structures functions (psfr.sf) and the scaled PSF in psfr.psf which is a *psfStats* object (see PUAKO note #04).

When called, the *psfReconstruction* executes the following steps

1. Call of the function *updateReconstructionPrerequisites* so as to define the sampling required in the different planes regarding the desired PSF field of view and detector pixel scale. If $\Delta\theta$ is the camera pixel scale in radian and Θ is the field of view in pixels the PSF must me reconstructed over, the OTF and pupil resolution, respectively $n_{\rm otf}$ and $n_{\rm pup}$, are derived as follows

$$\begin{aligned} \Delta k &= 2 \times n_{\rm act} - 1 \\ \text{Samp} &= \frac{\lambda}{2 \times D \times \Delta\theta} \\ n_{\rm ao} &= (n_{\rm act} - 1) \times \text{Samp} \\ n_{\rm T} &= \max(1, \text{round}(\Theta / n_{\rm ao})) \\ n_{\rm otf} &= 2 \times \text{floor}(\Delta k \times n_{\rm T}/2), \\ n_{\rm pup} &= n_{\rm otf}/2 \end{aligned} \tag{1}$$

   where Δk is the resolution of the AO corrected area in the spatial frequency domain, Samp the oversampling factor compared to the Nyquist sampling, $n_{\rm ao}$ the number of pixels the AO correction area is spread over in the focal-plane and $n_{\rm T}$ the ratio between the maximal spatial frequency and the DM cut-off frequency. Automatically, PUAKO will interpolate the telescope pupil model, static aberrations maps and DM influence functions at the new pupil resolution, as well as calculate the image Strehl-ratio and the diffraction-limit OTF.

2. Calculate all OTFs required in the reconstruction process using the *forwardPSFR* function: the static OTF, the fitting, the aliasing, the AO residual, the residual tip-tilt, the anisoplanatism and the CCD transfer function. The PSF is obtained from the FFT algorithm applied on the final OTF including any zero-padding or interpolation to derive the PSF at the appropriate pixel scale.

3. Scale the reconstructed PSF by fitting it on the on-sky image, i.e. retrieving the 2D astrometry, photometry and background if specified by the user. This step is performed by the *psfStats* object that takes care of calculating the Strehl-ratio, FWHM and any figures of merit of the reconstructed PSF.

In the following, I expend the derivation of all terms involved in the reconstruction.

3 PSF reconstruction framework

3.1 Theoretical background

The original PSFR framework proposed by [21] has been designed to estimate the long-exposure AO PSF from WFS measurements, DM commands and specific calibration, such as NCPA map or DM influence functions. I distinguish three fundamental hypothesis the current PSF reconstruction relies on

1. **Phase stationarity**. We assume that the residual phase in the pupil plane is spatially stationary, which supposes that its variance is invariant across the pupil. Empirical observations shows that pupil edges

effects exist, but according to [22, 12, 21], this assumption does not harm the reconstruction, i.e. this is not a limiting factor for science application. Practically, this assumption allows to split the PSF into a contribution due to static aberrations coming from the telescope and optical path and a contribution due to the residual turbulence. The OTF $\tilde{h}$, which depends on the angular frequency $\boldsymbol{u}/\lambda$ derives as follows [18]

$$\tilde{h}(\boldsymbol{\rho}/\lambda) = \tilde{h}_{\text{tel}}(\boldsymbol{\rho}/\lambda).\tilde{k}_{\text{atm}}(\boldsymbol{\rho}/\lambda).\tilde{k}_{\text{det}}(\boldsymbol{\rho}/\lambda), \tag{2}$$

where (i) $\tilde{h}_{\text{tel}}(\boldsymbol{\rho}/\lambda)$ is the static OTF including the pupil shape and static aberrations map, (ii) $\tilde{k}_{\text{atm}}$ is a spatial filter that characterizes the impact of the residual turbulence onto the PSF and (iii) $\tilde{k}_{\text{det}}$ is the detector transfer function.

2. **Gaussian distribution**. We assume that the residual atmospheric phase follows a zero-mean Gaussian distribution $\mathcal{N}(0, \sigma_\varepsilon^2)$ where σ_ε^2 is the AO residual wavefront error. Therefore, the spatial filter $\tilde{k}_{\text{atm}}$, **in the case of long-exposure PSF reconstruction**, depends on the residual phase 2nd order statistical moment only

$$\tilde{k}_{\text{atm}}(\boldsymbol{\rho}/\lambda) = \exp\left(-\frac{2\pi^2}{\lambda^2}\mathcal{D}_\varepsilon(\boldsymbol{\rho})\right), \tag{3}$$

where $\mathcal{D}_\varepsilon$ is the phase structure function of the residual OPD in the pupil.

3. **Statistical independence**. We assume that the residual OPD results from a sum of statistically independent terms, which are the DM fitting error, the aliasing, the AO residual error tip-tilt excluded, the residual tip-tilt and the anisoplanatism. Eventually we have

$$\mathcal{D}_\varepsilon(\boldsymbol{\rho}) = \mathcal{D}_\perp(\boldsymbol{\rho}) + \mathcal{D}_{\text{al}}(\boldsymbol{\rho}) + \mathcal{D}_{\text{tt}}(\boldsymbol{\rho}) + \mathcal{D}_{\text{ao}}(\boldsymbol{\rho}) + \mathcal{D}_\Delta(\boldsymbol{\rho}). \tag{4}$$

Therefore, PSF reconstruction consists in calculating the static OTF $\tilde{h}_{\text{tel}}$ from static aberrations calibration, modeling the detector response $\tilde{k}_{\text{det}}$ and deriving all structure functions in Eq. 4.

3.2 Static OTF

We define $\delta_{\text{stat}}(\theta)$ as the calibrated static aberrations map expressed in nm. It contains four different contributors that depends on the coordinates in the pupil $\boldsymbol{r}$ and the direction in the field θ

$$\begin{aligned} \delta_{\text{stat}}(\boldsymbol{r}, \theta) &= \delta_{\text{calib}}(\boldsymbol{r}, \theta) + \sum_i^{n_{\text{m}}} a_i Z_i(\boldsymbol{r}) \\ \delta_{\text{calib}}(\boldsymbol{r}, \theta) &= \delta_{\text{ncpa}}(\boldsymbol{r}) + \delta_{\text{diff}}(\boldsymbol{r}, \theta) + \delta_\perp(\boldsymbol{r}) \end{aligned} \tag{5}$$

where

- δ_{ncpa} results from the NCPA calibration, generally done at the beginning of the night. See [16, 17] to learn about the calibration process.
- δ_{diff} is the differential field-dependent static aberrations that depends on where the PSF is on the detector plane. This term is deduced from field-dependent static calibrations done in 2014 [19] using the internal fiber on the Keck II AO bench. Thanks to this work, we have a static aberration map every 1" in the 10"×10" NIRC2 field (so 81 maps in total). Thus, when instantiating the *telemetry* object, PUAKO will call the function *differentialStaticAberrations* that (i) extracts the four (can be changed with the optional parameter `nWeight`) closest maps from the PSF position in the detector plane (which is estimated in

the function *processDetectorImage* and extrapolate the map at the position θ using the inverse distance weighting, (ii) repeat the same operation for estimating the static map at the position the NCPA has been calibrated on-sky. **Warning:** by default, the algorithm will assume that the calibration has been made on-axis if there is no way to retrieve this information. I suggest to put the PSF coordinates (10 pixels accuracy is enough) during the NCPA calibration in the scientific image fits header, or to grant access to the raw image that have served to calibrate the NCPA. Note that PUAKO does not perform any phase retrieval, it is the responsibility of the user to provide this map or not and (iii) define δ_{diff} as the difference between the two extrapolated maps. Note that field-dependent calibration have not been performed on-sky yet, so we assume that the telescope does not change the static aberrations variability, which is an assumption and I'd like to verify.

- $\delta_{\perp}$ is the map of high spatial frequency static aberrations in the optical path and is assumed to be constant in the field and time invariant. See [16] to learn more about the calibration of this term.

- a_i and Z_i are respectively the coefficients and modes of any polynomial aberrations we want to include on top of calibrations. Only constrains are that a_i must be given in nm and Z_i must be given as a column-vector. The user can provide a combination of any modes using the `addStatModes` property.

Field-dependent and high-order aberrations are reconstructed over a circular pupil ('INCIRCLE' mask), while the NCPA is calibrated using the 'OPEN' NIRC2 mask (hexagonal pupil). To model the pupil, PUAKO reads the scientific image fits header to extract the corresponding keyword and three options are available (i) 'LARGEHEX' to model the pupil with a hexagonal shape extruded by a hexagonal obstruction (ii) 'INCIRCLE' to model the pupil with an annular shape (iii) 'OPEN' to model the complete segmented Keck pupil, either from a high-resolution synthetic image interpolated at the n_{tel} resolution or from the logical values of the NCPA calibration map. The three models are represented in Fig. 1.

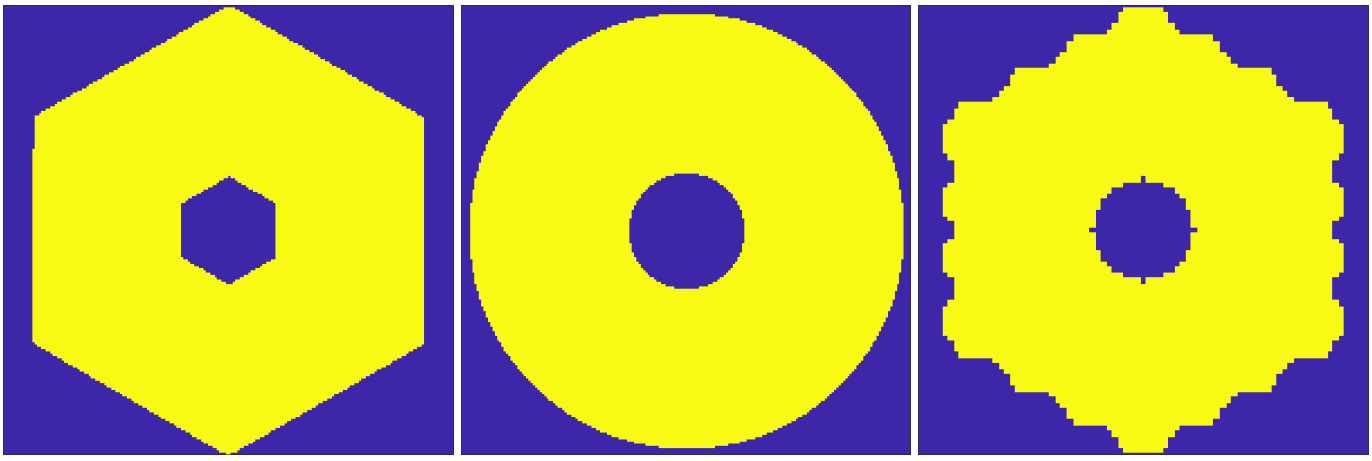

Figure 1: Pupil models implemented into PUAKO. From left to right: hexagonal (*LargeHex.sav*: A = 1.301 m and B = 5.328 m), annular (the outer diameter is 9.98 m and the inner diameter is 2.65 m) and open shapes. The last one is derived from the NCPA calibration map.

From the pupil model, PUAKO calculates the diffraction-limit OTF from

$$\tilde{h}_{\text{DL}}(\boldsymbol{\rho}/\lambda) = \iint_{\mathcal{P}} \mathcal{P}(\boldsymbol{r})\mathcal{P}^{*}(\boldsymbol{r}+\boldsymbol{\rho})\boldsymbol{dr}, \tag{6}$$

that serves the calculation of Strehl-ratio in the error breakdown derivation (see PUAKO notes #05). PUAKO finally derives the static OTF that appears in Eq. 2 from δ_{stat} as follows

$$\tilde{h}_{\text{tel}}(\boldsymbol{\rho}/\lambda, \theta) = \iint_{\mathcal{P}} \mathcal{P}(\boldsymbol{r})\mathcal{P}^*(\boldsymbol{r}+\boldsymbol{\rho}) \exp\left(-\frac{2i\pi}{\lambda}\left(\delta_{\text{stat}}(\boldsymbol{r}, \theta) - \delta_{\text{stat}}(\boldsymbol{r}+\boldsymbol{\rho}, \theta)\right)\right). \tag{7}$$

3.3 Fitting phase structure function

The fitting phase structure function is determined thanks to an analytical model that depends on the r_0 and L_0 (this latter should have a lesser, even none, influence). Function $\mathcal{D}_\perp$ is calculated from the fitting covariance function $C_\perp$ which is derived from the Von-Kármánn PSD of the atmospheric phase $\mathcal{W}_\phi$ as follows

$$\begin{aligned}
\mathcal{D}_\perp(\boldsymbol{\rho}) &= 2 \times (C_\perp(\mathbf{0}) - C_\perp(\boldsymbol{\rho})) \\
C_\perp(\boldsymbol{\rho}) &= \iint_{\mathcal{R}^2} \mathcal{W}_\phi(\boldsymbol{k}).\Pi_{k_c}(\boldsymbol{k}) \\
\mathcal{W}_\phi(\boldsymbol{k}) &= 0.0229 \times r_0^{-5/3}\left(k^2 + \frac{1}{L_0^2}\right)^{-11/6},
\end{aligned} \tag{8}$$

where Π_{k_c} is the spatial filter mask that depends on the DM cut-off frequency k_c. SO far, there are two masks implemented (and tested) on PUAKO, which are the circle and square masks

$$\begin{aligned}
\Pi_{k_c}^{\text{square}}(k) &= \begin{cases} 0 & \text{if} \quad k_x \leq k_c \text{ or } k_y \leq k_c \\ 1 & \text{else} \end{cases} \\
\Pi_{k_c}^{\text{circle}}(k) &= \begin{cases} 0 & \text{if} \quad \sqrt{k_x^2 + k_y^2} \leq k_c \\ 1 & \text{else} \end{cases}
\end{aligned} \tag{9}$$

By default, the mask is set up to the circular one. The real AO correction pattern should depend on the number of controlled modes and the DM influence functions, especially on the slaved actuators at the pupil edges. I did not manage to implement this facility so far but it is envisioned for later upgrade.

3.4 Aliasing phase structure function

Similarly as the fitting structure function, the aliasing structure function depends straightforwardly on the aliasing PSD $\mathcal{W}_{\text{al}}$ [6, 11, 8] that accounts for the spatial filtering of the Shack-Hartmann WFS and the temporal propagation of the aliased measurement through the AO loop. Eventually we have

$$\mathcal{W}_{\text{al}}(\boldsymbol{k}) = \frac{0.0229 r_0^{-5/3}}{4\text{sinc}\,(\boldsymbol{k}d)} \times \sum_{\substack{p=-\zeta \\ p\neq 0}}^{\zeta} \sum_{\substack{q=-\zeta \\ q\neq 0}}^{\zeta} \sum_{l=1}^{n_{\text{L}}} f_l \frac{(\boldsymbol{k}^{-1}.\boldsymbol{k}_{pq})^2 \text{sinc}\left(k_p d\right) \text{sinc}\left(k_q d\right)}{\left(k^2 + 1/L_0(l)^2\right)^{11/6}} . \mathcal{H}_{\text{cl}}(l), \tag{10}$$

with

$$\mathcal{H}_{\text{cl}}(l) = \frac{g^2 \text{sinc}\left(k_p v_{lx} t_i\right) \text{sinc}\left(k_q v_{ly} t_i\right) \exp(2i\pi(k_p v_{lx} + k_q v_{ly}) t_d)}{1 - 2(\iota - g)\cos\left(2\pi k_p v_{lx} t_i\right)\cos\left(2\pi k_q v_{ly} t_i\right) + (\iota - g)^2} \tag{11}$$

and where

- d the sub-aperture size and $\mathcal{H}_{\text{cl}}(l)$ is the temporal rejection function of the loop, that is spatialized by replacing temporal frequencies with $\boldsymbol{f} = \boldsymbol{k}.\boldsymbol{v}_l$ where $\boldsymbol{v}_l$ is the velocity vector (norm is the windspeed value, angle is the wind direction) of the l^{th} layer.

- $\boldsymbol{k}_{pq} = (k_p, k_q)$ with $k_p = k_x - p/d$ and $k_q = k_y - q/d$ as the x/y frequency vectors shifted by respectively p/d and q/d.
- ζ is a unitless number defined by the highest frequency seen by the WFS normalized by the DM cut-off frequency k_{AO}. This number accounts for the spatial filtering in the WFS optical path that has been implemented to mitigate as much as possible the aliasing effect [15].
- $v_{lx} = v_l \cos(\omega_l)$ and $v_{ly} = v_l \sin(\omega_l)$ are the components of the velocity vector at height h_l, projected respectively on the x-axis and y-axis of the frequency plan, with v_l, ω_l the corresponding turbulence velocity and wind direction values at height h_l.
- $L_0(l)$ is the outer scale vertical profile. Practically, we have chosen a flat profile and $L_0 = 25$, but methods exist to retrieve the integrated outer scale value from the telemetry [1].
- t_i and t_d are respectively the WFS temporal sampling frequency and the loop delay, that is 2.3 frames .
- g is the average of modal gain vector [14]. To be more accurate, we should evaluate how the WFS aliasing propagate through each controlled KL mode and though the AO loop by taking into account the modal optimization. However such a description would drastically increase the complexity of the aliasing PSD computation for a small improvement eventually.
- ι is the integrator leak factor set to 1 (no leak) in the rest of this paper.

3.5 Tip-tilt phase structure function

The residual tip-tilt is assumed to convolve the PSF by an asymmetric Gaussian function that depends on three parameters. The first thing to manage is the pupil orientation that can be different between the telescope and WFS pupil-planes by a rotation angle ψ that is defined from two keywords in the fits header and the telescope elevation angle γ as follows

$$\psi = \mathrm{ROTPOSN} - \gamma - \mathrm{INSTANGL}. \tag{12}$$

On top of that, we now that there is a fixed rotation angle of 90° between the WFS and NIRC2 pupil. Eventually, we redefine the new components of the separation vector (from $-D/2$ to $D/2$) from

$$\begin{bmatrix} \omega_x \\ \omega_y \end{bmatrix} = \begin{bmatrix} \cos(\pi/2 + \psi) & -\sin(\pi/2 + \psi) \\ \sin(\pi/2 + \psi) & \cos(\pi/2 + \psi) \end{bmatrix} \begin{bmatrix} \rho_x \\ \rho_y \end{bmatrix} \tag{13}$$

$$\mathcal{D}_{tt}(\boldsymbol{\rho}) = \frac{4\pi^2}{\lambda^2 D^2} \left(\sigma_x^2 \boldsymbol{\omega}_x^2 + \sigma_y^2 \boldsymbol{\omega}_y^2 + 2\sigma_{xy}^2 \boldsymbol{\omega}_x \boldsymbol{\omega}_y \right). \tag{14}$$

The tip-tilt structure function is therefore calculated as a Gaussian function by taking the variance of the measured tip-tilt signal from the dedicated WFS to which we subtract the estimated noise variance (see PUAKO note #02)

$$\begin{aligned} \sigma_x^2 &= \frac{1}{n_{\mathrm{F}}} \sum_{t=1}^{n_{\mathrm{F}}} (\boldsymbol{u}_{\mathrm{tip}}(t) - \bar{\boldsymbol{u}}_{\mathrm{tip}})^2 - \sigma_{\eta_{\mathrm{tip}}}^2 \\ \sigma_y^2 &= \frac{1}{n_{\mathrm{F}}} \sum_{t=1}^{n_{\mathrm{F}}} (\boldsymbol{u}_{\mathrm{tilt}}(t) - \bar{\boldsymbol{u}}_{\mathrm{tilt}})^2 - \sigma_{\eta_{\mathrm{tilt}}}^2, \end{aligned} \tag{15}$$

where n_{F} is the number of exposure of the tip-tilt WFS, $\bar{u}$ the temporal average of u and $\boldsymbol{u}_{\mathrm{tip}}$ and $\boldsymbol{u}_{\mathrm{tip}}$ are converted in nm from the tip-tilt DM commands and using the conversion factor 12.68 μm/arcsec in NGS [20] and 40.6 μm/arcsec using STRAP in LGS mode (calibration with PRIME).

3.6 AO residual phase structure function

Methodology for estimating $\mathcal{D}_{\rm ao}$ from WFS measurements is highly spread in the literature [3, 16, 12, 10, 21]. Practically, PUAKO relies on the Vii algorithm proposed by [9] to speed up significantly the covariance calculation where

$$\mathcal{D}_{\rm ao}(\boldsymbol{\rho}) = \sum_{i}^{n_{\rm act}} \Lambda(i,i) V_{ii}(\boldsymbol{\rho}), \tag{16}$$

being V_{ii} the Vii functions obtained from the eigen decomposition of the matrix of the High-order DM influence functions, while Λ is the diagonal matrix that contains the eigenvalues of the covariance matrix $C_{\rm ao}$ of the residual phase. This later is calculated in the DM actuators space in meter using the conversion factor $0.4095\,\mu$m/V and the reconstructed wavefront $\boldsymbol{u}(t)$ that is stored in the telemetry recording system (field A. RESIDUALWAVEFRONT) as follows

$$C_{\rm ao} = \frac{4\pi^2}{\lambda^2 n_{\rm F}} \sum_{t=1}^{n_{\rm F}} (\boldsymbol{u}(t) - \bar{\boldsymbol{u}}).(\boldsymbol{u}(t) - \bar{\boldsymbol{u}})^t - C_\eta, \tag{17}$$

where C_η is the noise covariance matrix estimated at a previous stage (see PUAKO note #02). The Vii implementation within PUAKO follows instructions given in [9] and can be found in the function *modes2Otf*. This piece of code can also deploy the original Véran's Uij method [21] (much more longer, I do not recommend this one for large degrees of freedom systems) as well as the zonal calculation [10]. This latter looks to give marginally better results with two possible modes: high-resolution mode for which the DM influence functions are sampled at the pupil resolution (takes one up to few minutes of calculation instead of 10 seconds) and a low-resolution ($2n_{\rm act}$ + 1 pixels to describe the influence functions) mode that is as fast as the Vii method. The interest of the Vii approach is that we have directly the phase structure function Toeplitz map (not the 4D matrix), which avoid recalculating either the map from the 4D matrix or the point-wise AO residual OTF in each iteration of PRIME (see PUAKO note #04), so we save a significant amount of time.

3.7 Anisoplanatism phase structure function

The anisoplanatism calculation can be found in the function *computeAnisoplanatismPhaseStrcutureFunction* in which $\mathcal{D}_\Delta$ is derived as follows

$$\mathcal{D}_\Delta(\boldsymbol{\rho}) = \mathrm{P}_{\rm TTR}\mathcal{D}_{\Delta{\rm lgs}}(\boldsymbol{\rho})\mathrm{P}_{\rm TTR}^t + \mathrm{P}_{\rm TT}\mathcal{D}_{\Delta{\rm ngs}}(\boldsymbol{\rho})\mathrm{P}_{\rm TT}^t \tag{18}$$

where $\mathcal{D}_{\Delta{\rm lgs}}$ /$\mathcal{D}_{\Delta{\rm ngs}}$ is the anisoplanatic structure function of the differential atmospheric phase between the LGS (cone effect included)/NGS and scientific target directions and $\mathrm{P}_{\rm TTR}$/$\mathrm{P}_{\rm TT}$ is a filtering matrix that remove the tip-tilt/high-order modes. This is assuming that the total anisoplanatism results from the sum of the angular-focal plus tip-tilt anisoplanatism, which a reasonable approximation [2]. Moreover, this model does not account for any possible cross-correlation between temporal and anisoplanatism effects that may occur if there is a single very fast, energetic and high layer [7] simultaneously. As long as the C_n^2 and turbulence velocity profiles are distributed in a quite smooth fashion, such an effect should not be noticeable.
There two different ways to get the anisoplanatic structure function (i) using the covariance-based framework proposed [4] or (ii) use the analytical expression from [8]. Both are giving very similar results [2]. Regardless the method, the calculation relies on the C_n^2 profile that is identified from the MASS-DIMM if data available or from Mauna Kea median conditions if not. Finally, the C_n^2 profile is scaled to obtain an integrated seeing value along the line of sight equal to the seeing identified from the telemetry (see PUAKO notes #02).

3.8 CCD transfer function

The CCD transfer function is modeled simply as follows

$$\tilde{k}_{\text{det}}(\boldsymbol{\rho}/\lambda) = \text{sinc}(\rho_x \Delta\theta/\lambda).\text{sinc}(\rho_y \Delta\theta/\lambda) \tag{19}$$

which permits to convolve the PSF by a pixel-sized gate function. This model does not account for any CCD diffusion or other effects that may enlarge the pixel response. So as to improve this model (if it's necessary but I do not think so), we could assume that the pixel response is a Gaussian of FWHM corresponding to the pixel scale (9.94 mas in the NIRC2 narrow field mode) for instance, which can be verified by testing the current PSF reconstruction pipeline on laboratory data with in a controlled environment.

4 Application to Keck data

I have launched an automatic PSF reconstruction overall the 304 data sets acquired during four different observing nights. Statistically, processing a NGS data set takes less than 20 s including 15 s for the reconstruction plus fit (astrometry/photometry) on the image and for a high-resolution sampling (the PSF is calculated over twice the reference image). For LGS data, PUAKO must include the anisoplanatism calculation so it takes more like 30 s in total and 20 s for the reconstruction.

I present in Fig. 3 and Fig. 2 successful reconstruction in both NGS and LGS modes, with different seeing and windshake conditions. Oddly, the PSF FWHM in LGS mode was near to 60 mas while the diffraction in K is more like 40 mas. There is an jitter excess that can be retrieved from the telemetry as long as we use a conversion factor of 40.6 μm/arcsec for calibrating the optical gain of STRAP. Strehl-ratio is quite well reconstructed and correlated with measurements, but FWHM estimates is much more dispersed, particularly in LGS mode. I did not identified so far whether it comes from calibration issues (differential gain x/y axis for STRAP ?), pupil rotation model (no rotation in NGS mode in the data I have processed) or any static aberrations missing. We particularly notice that the LGS PSF is quite asymmetric for this observing night and the residual is mainly dominated by a smooth pattern, i.e. I do not really suspect any troubles with NCPA calibration. The facts that the system was not working as efficiently as expected and the PSF reconstruction is not as accurate as in NGS mode are maybe connected, which can be the case if the WFSs does not behave as we model them. I can not give clear hints on the origin of this mis-performance, but I believe that applying PSF reconstruction is a good step to stat diagnosing the system.

In Fig. 5, I present the Fraction of Variance Unexplained (FVU) [13], which is a normalized mean square error actually, obtained by adjusting astrometry/photometry on the image PSF using either the reconstructed PSF or a Gaussian model. Systematically, using the reconstructed PSF allows to decrease the fitting residual, which claims for a better PSF representation comparatively to the Gaussian model. Statistically overall the 304 data sets, we have a factor two improvement on this metrics, which signifies roughly that each pixels of the residual map is twice lower using the reconstructed PSF than the Gaussian model. Note that the Gaussian model is calibrated using directly the focal-plane image while the reconstruction utilizes the AO telemetry only. As a conclusion, PUAKO permits to obtain a more accurate PSF representation without using the focal-plane image than a Gaussian model.
Besides improving our knowledge of the system and enrich the reconstruction mode, there is a way to get beyond those results by using hybrid PSF reconstruction combining AO telemetry and focal-plane image as I present in the PUAKO note #04.

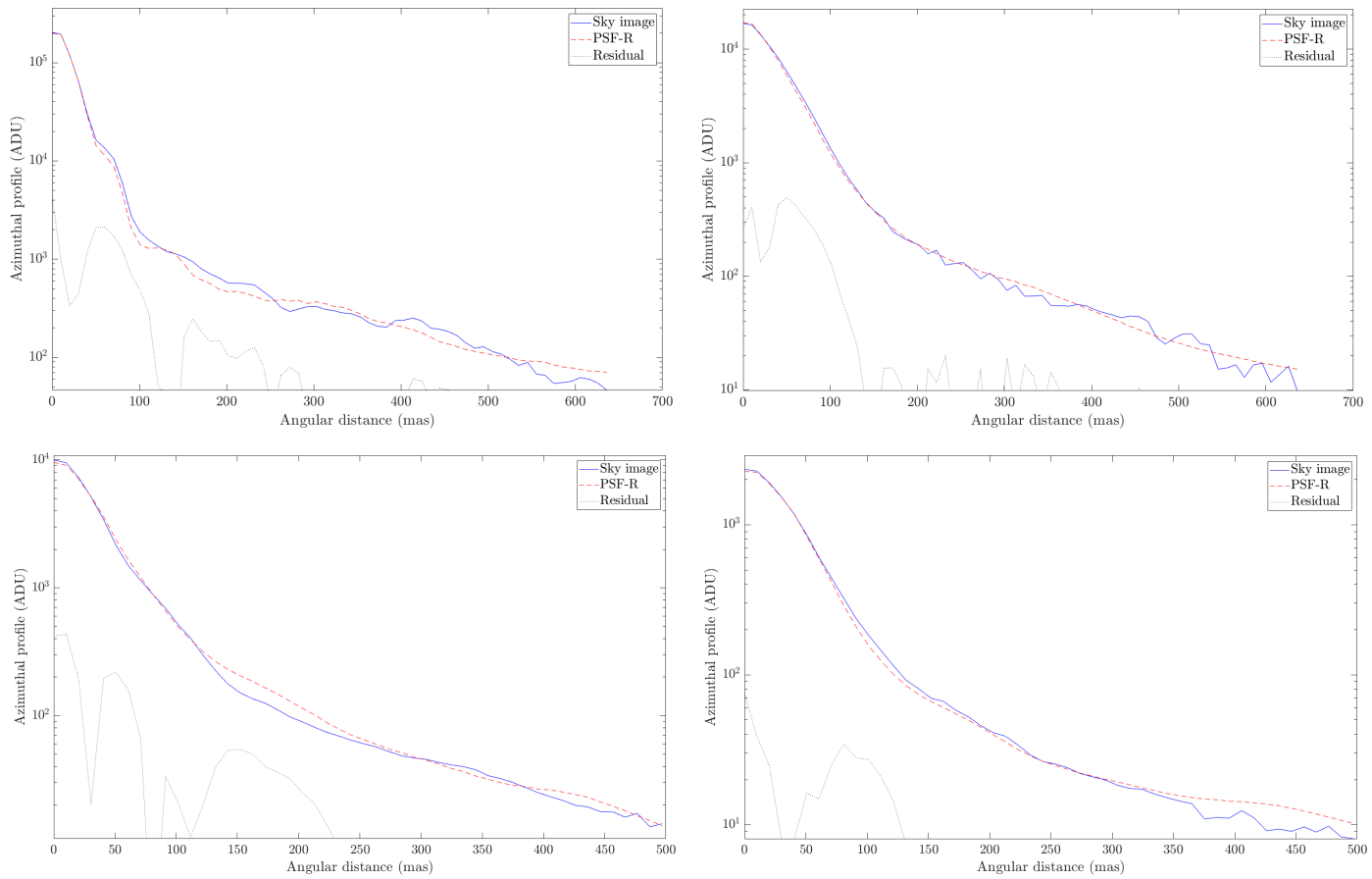

Figure 2: Azimuthal profiles obtained on the sky, reconstructed or and residual PSF for two different data set (top-left: n0004-NGS, top-right: n0070-NGS, bottom-left: n0030-LGS, bottom-right: n0125-LGS) acquired on August 1st 2013 (NGS) and March 14th 2017 (LGS).

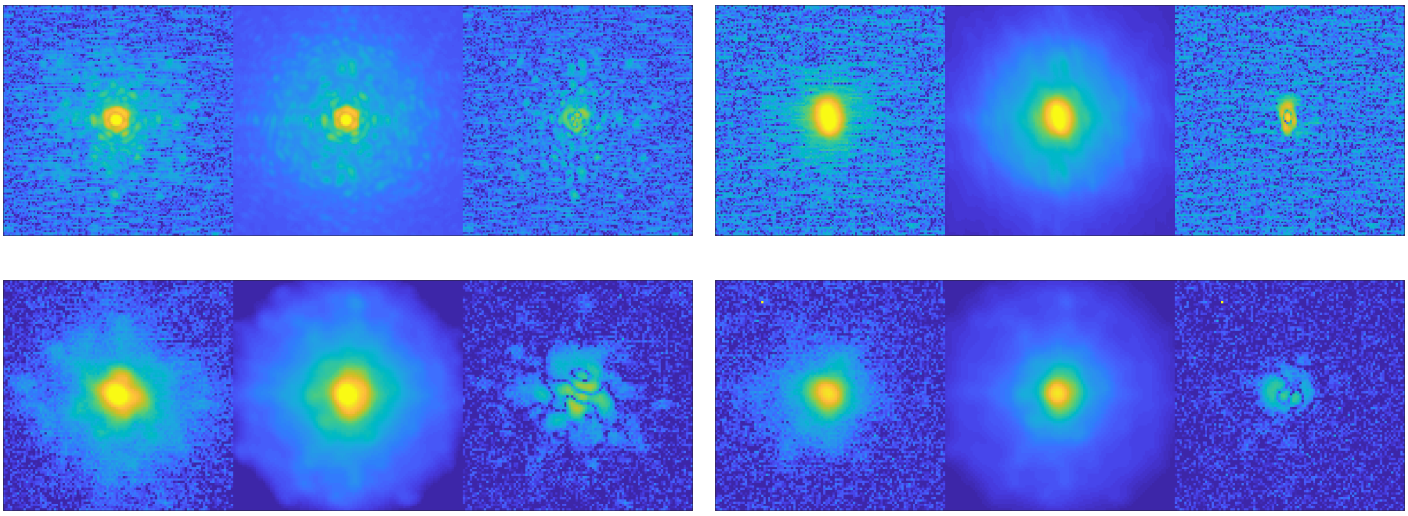

Figure 3: 2D on-sky (left), reconstructed (middle) and residual (right) image for two different data set (top-left: n0004-NGS, top-right: n0070-NGS, bottom-left: n0030-LGS, bottom-right: n0125-LGS) acquired on August 1st 2013 (NGS) and March 14th 2017 (LGS).

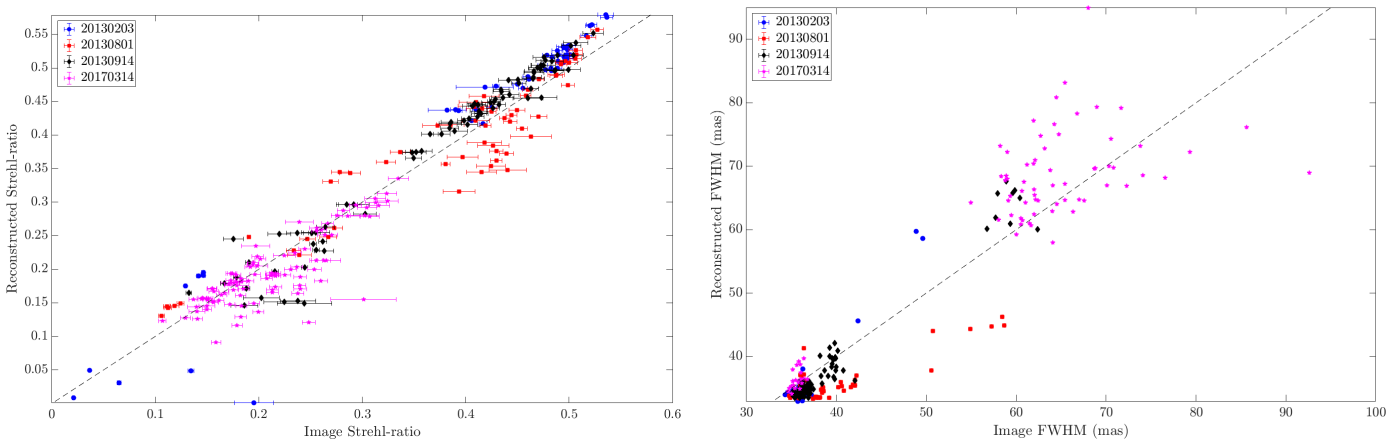

Figure 4: Reconstructed metrics (left: Strehl-ratio, right: FWHM) versus image measurements sorted by acquisition date.

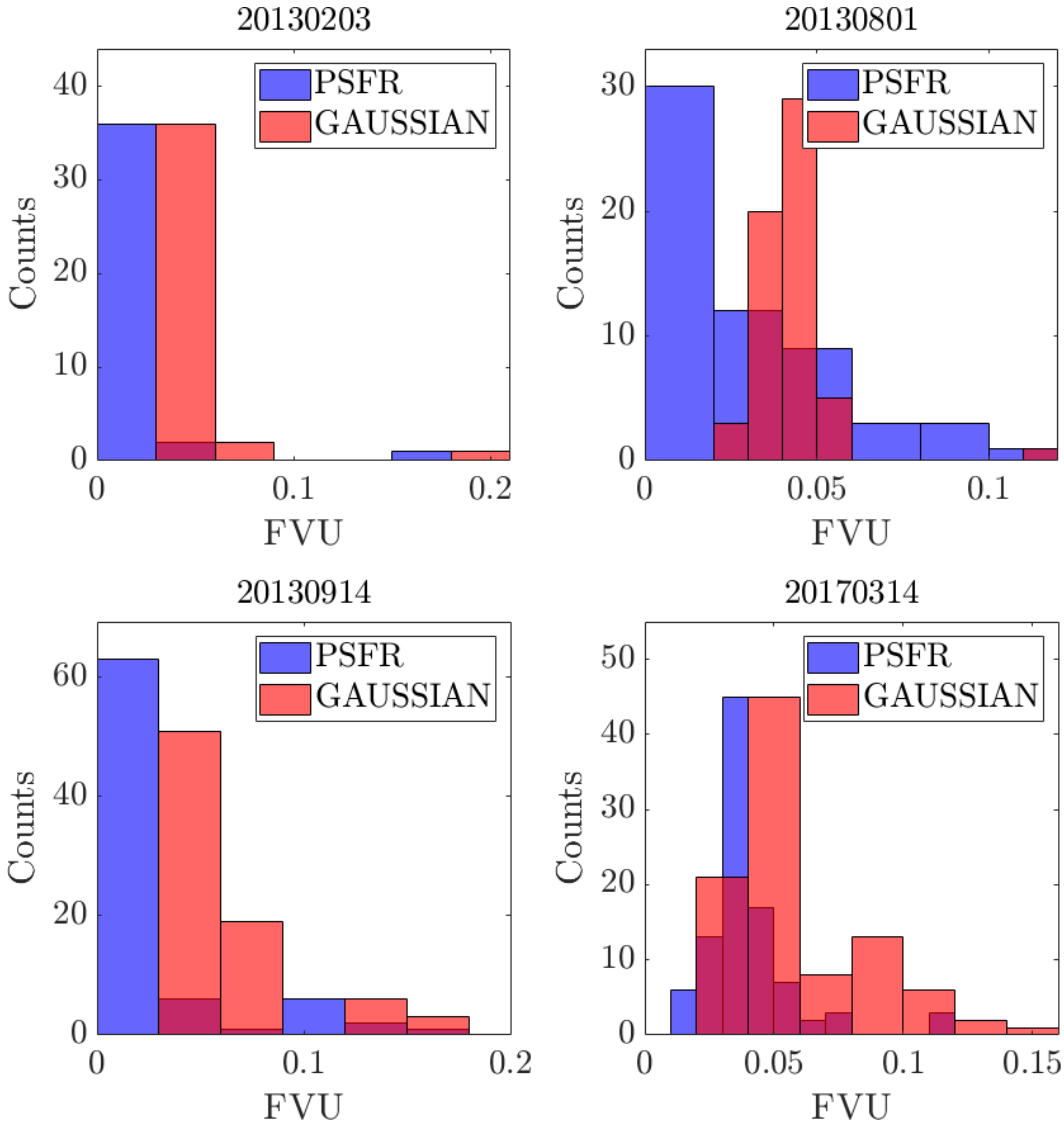

Figure 5: Fraction of Variance Unexplained obtained after comparing either the reconstructed PSF or a Gaussian model with the sky image.

References

[1] Paulo P. Andrade, Paulo J. V. Garcia, Carlos M. Correia, Johann Kolb, and Maria Inês Carvalho. Estimation of atmospheric turbulence parameters from Shack-Hartmann wavefront sensor measurements. *M.N.R.A.S* , 483(1):1192–1201, Feb 2019.

[2] O. Beltramo-Martin, C. M. Correia, E. Mieda, B. Neichel, T. Fusco, G. Witzel, J. R. Lu, and J.-P. Véran. Off-axis point spread function characterization in laser guide star adaptive optics systems. *M.N.R.A.S* , 478:4642–4656, August 2018.

[3] O. Beltramo-Martin, C. M. Correia, S. Ragland, L. Jolissaint, B. Neichel, T. Fusco, and P. L. Wizinowich. PRIME: PSF Reconstruction and Identification for Multiple-source characterization Enhancement - application to Keck NIRC2 imager. *M.N.R.A.S* , 487(4):5450–5462, Aug 2019.

[4] R. Conan, J. Borgnino, A. Ziad, and F. Martin. Analytical solution for the covariance and for the decorrelation time of the angle of arrival of a wave front corrugated by atmospheric turbulence. *Journal of the Optical Society of America A*, 17:1807–1818, October 2000.

[5] R. Conan, A. Ziad, J. Borgnino, F. Martin, and A. A. Tokovinin. Measurements of the wavefront outer scale at Paranal: influence of this parameter in interferometry. In P. Léna and A. Quirrenbach, editors, *Interferometry in Optical Astronomy*, volume 4006 of *Proc. SPIE* , pages 963–973, July 2000.

[6] C. M. Correia and J. Teixeira. Anti-aliasing Wiener filtering for wave-front reconstruction in the spatial-frequency domain for high-order astronomical adaptive-optics systems. *Journal of the Optical Society of America A*, 31:2763, December 2014.

[7] F. Ferreira, E. Gendron, G. Rousset, and D. Gratadour. Numerical estimation of wavefront error breakdown in adaptive optics. *Astron. & Astrophys.* , 616:A102, August 2018.

[8] R Flicker. PSF reconstruction for Keck AO. Technical report, W.M. Keck Observatory, 65-1120 Mamalahoa Hwy, Waimea, HI 96743, United-States, 2008.

[9] E. Gendron, Y. Clénet, T. Fusco, and G. Rousset. New algorithms for adaptive optics point-spread function reconstruction. *Astron. & Astrophys.* , 457:359–363, October 2006.

[10] Luc Gilles, Carlos Correia, Jean-Pierre Véran, Lianqi Wang, and Brent Ellerbroek. Simulation model based approach for long exposure atmospheric point spread function reconstruction for laser guide star multiconjugate adaptive optics. *Appl. Opt.*, 51(31):7443–7458, Nov 2012.

[11] L. Jolissaint. Synthetic modeling of astronomical closed loop adaptive optics. *Journal of the European Optical Society - Rapid publications, 5, 10055*, 5, November 2010.

[12] L. Jolissaint, S. Ragland, and P. Wizinowich. Adaptive Optics Point Spread Function Reconstruction at W. M. Keck Observatory in Laser Natural Guide Star Modes : Final Developments. In *Adaptive Optics for Extremely Large Telescopes IV (AO4ELT4)*, page E93, October 2015.

[13] I. R. King. Accuracy of measurement of star images on a pixel array. *Publications of the Astronomical Society of the Pacific* , 95:163–168, February 1983.

[14] Cyril Petit, Thierry Fusco, Julien Charton, David Mouillet, Patrick Rabou, Tristan Buey, Gérard Rousset, Jean-François Sauvage, Pierre Baudoz, and Pierre Gigan. The SPHERE XAO system: design and performance. In *Adaptive Optics Systems*, volume 7015 of *Proc. SPIE* , page 70151U, Jul 2008.

[15] Lisa A. Poyneer, Brian Bauman, Bruce A. Macintosh, Daren Dillon, and Scott Severson. Experimental demonstration of phase correction with a 32×32 microelectromechanical systems mirror and a spatially filtered wavefront sensor. *Optics Letters*, 31(3):293–295, Feb 2006.

[16] S. Ragland, T. J. Dupuy, L. Jolissaint, P. L. Wizinowich, J. R. Lu, M. A. van Dam, G. B. Berriman, W. Best, C. R. Gelino, A. M. Ghez, M. C. Liu, J. A. Mader, A. Vayner, G. Witzel, and S. A. Wright. Status of point spread function determination for Keck adaptive optics. In *Adaptive Optics Systems VI*, volume 10703 of *Proc. SPIE* , page 107031J, July 2018.

[17] S. Ragland, L. Jolissaint, P. Wizinowich, M. A. van Dam, L. Mugnier, A. Bouxin, J. Chock, S. Kwok, J. Mader, G. Witzel, T. Do, M. Fitzgerald, A. Ghez, J. Lu, G. Martinez, M. R. Morris, and B. Sitarski. Point spread function determination for Keck adaptive optics. In *Adaptive Optics Systems V*, volume 9909 of *Proc. SPIE* , page 99091P, July 2016.

[18] F. Roddier. The effects of atmospheric turbulence in optical astronomy. *Progress in optics. Volume 19. Amsterdam, North-Holland Publishing Co., 1981, p. 281-376.*, 19:281–376, 1981.

[19] B. N. Sitarski, G. Witzel, M.P. Fitzgerald, L. Meyer, A. M. Ghez, R. D. Campbell, J. R Lu, K. Matthews, P. Wizinowich, and J. Lyke. Modeling instrumental field-dependent aberrations in the nirc2 instrument on the keck ii telescope. In *Adaptive Optics Systems IV*, volume 9148 of *Proc. SPIE* , August 2014.

[20] Marcos A. van Dam, David Le Mignant, and Bruce A. Macintosh. Performance of the Keck Observatory Adaptive-Optics System. *Applied Optics*, 43(29):5458–5467, Oct 2004.

[21] J.-P. Veran, F. Rigaut, H. Maitre, and D. Rouan. Estimation of the adaptive optics long-exposure point-spread function using control loop data. *Journal of the Optical Society of America A*, 14:3057–3069, November 1997.

[22] R. Wagner, C. Hofer, and R. Ramlau. Point spread function reconstruction for single-conjugate adaptive optics on extremely large telescopes. *J. of Astronomical Telescopes, Instruments, ans Systems*, 4(4):049003, 2018.